Available online at www.sciencedirect.com
SCIENCE DIRECT®
Journal of Power Sources 128 (2004) 76–89
JOURNAL OF POWER SOURCES
www.elsevier.com/locate/jpowsour

Models of energy sources for EV and HEV: fuel cells, batteries, ultracapacitors, flywheels and engine-generators

Joeri Van Mierlo[a,*], Peter Van den Bossche[b,1], Gaston Maggetto[a,2]

[a] *Vrije Universiteit Brussel, ETEC-tw-VUB, Pleinlaan 2, 1050 Brussels, Belgium*
[b] *CITELEC, ETEC-tw-VUB, Pleinlaan 2, 1050 Brussels, Belgium*

Received 8 January 2003; received in revised form 12 August 2003; accepted 8 September 2003

Abstract

Resulting from a Ph.D. research a Vehicle Simulation Programme (VSP) is proposed and continuously developed. It allows simulating the behaviour of electric, hybrid, fuel cell and internal combustion vehicles while driving any reference cycle [Simulation software for comparison and design of electric, hybrid electric and internal combustion vehicles with respect to energy, emissions and performances, Ph.D. Thesis, Department Electrical Engineering, Vrije Universiteit Brussel, Belgium, April 2000]. The goal of the simulation programme is to study power flows in vehicle drive trains and the corresponding component losses, as well as to compare different drive train topologies. This comparison can be realised for energy consumption and emissions as well as for performances (acceleration, range, maximum slope, etc.).

The software package and its validation are described in [J. Automot. Eng., SAE IEE 215 (9) (2001) 1043L]. Different hybrid and electric drive trains are implemented in the software [Views on hybrid drive train power management strategies, in: Proceedings of the EVS-17, Montreal, Canada, October 2000]. The models used for the energy sources like fuel cells, batteries, ultracapacitors, flywheels and engine-generator units will be discussed in this paper in three stages: first their functionality and characteristics are described, next the way these characteristics can be implemented in a simulation model will be explained and finally some calculation results will illustrate the approach.

This paper is aimed to give an overview of simulation models of energy sources for battery, hybrid and fuel cell electric vehicles. Innovative is the extreme modularity and exchangeability of different components functioning as energy sources. The unique iteration algorithm of the simulation programme allows to accurately simulate drive train maximum performances as well as all kind of power management strategies in different types of hybrid drive trains [IEEE Trans. Veh. Technol., submitted for publication].

Keywords: Simulation; Fuel cell; Energy storage; Battery model; HEV

1. Introduction

The pollution caused by transport is a heavy burden, especially in urban areas [5]. The introduction of clean vehicles, like electrically driven vehicles, would be an interesting move in the direction of a significant reduction in harmful exhaust gases, with a view to a sustainable transport policy [6]. Since several years the family of the battery electric vehicles is extended with the hybrid electric and recently also with the fuel cell electric vehicles. These vehicle technologies use different energy sources, which will be discussed in this paper.

The energy sources that will be considered in this manuscript are mainly used in "series" hybrid vehicles. In series hybrid drives there are no mechanical connections between the internal combustion engine and the wheels [7]. All thermal energy is converted first into mechanical energy in a thermal engine and subsequently into electrical energy by a generator driven by the thermal engine. Additionally, there is an electric traction motor to drive the wheels. Hence a decoupling of energy source operation from the required traction power is possible. In most cases the energy source, also called auxiliary power unit (APU), will act as base power unit delivering power to the battery or directly to the electric traction motor. While driving the battery acts as peak power unit or energy buffer. The series hybrid has the advantage of operating a thermal engine in a selected optimal operating field, for instance, with low specific fuel consumption in the torque-speed operating area [8].

The fuel cell hybrid structure is a series structure in which the engine and the generator are replaced by a fuel cell

* Corresponding author. Tel.: +32-2-6292839; fax: +32-2-6293620.
E-mail addresses: jvmierlo@vub.ac.be (J. Van Mierlo), pvdbos@vub.ac.be (P. Van den Bossche), gmagget@vub.ac.be (G. Maggetto).
URLs: http://etecnts1.vub.ac.be/vsp/, http://www.citelec.org.
[1] Tel.: +32-2-6293807; fax: +32-2-6293620.
[2] Tel.: +32-2-6292804; fax: +32-2-6293620.

0378-7753/$ – see front matter © 2003 Elsevier B.V. All rights reserved.
doi:10.1016/j.jpowsour.2003.09.048

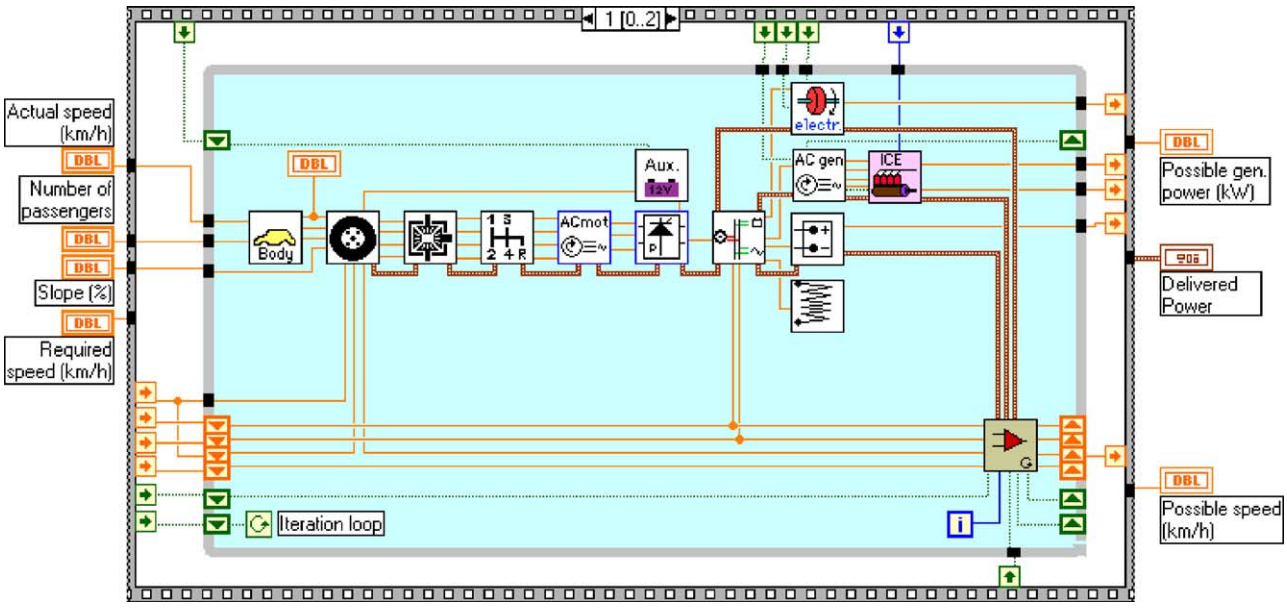

Fig. 1. Series hybrid drive train model.

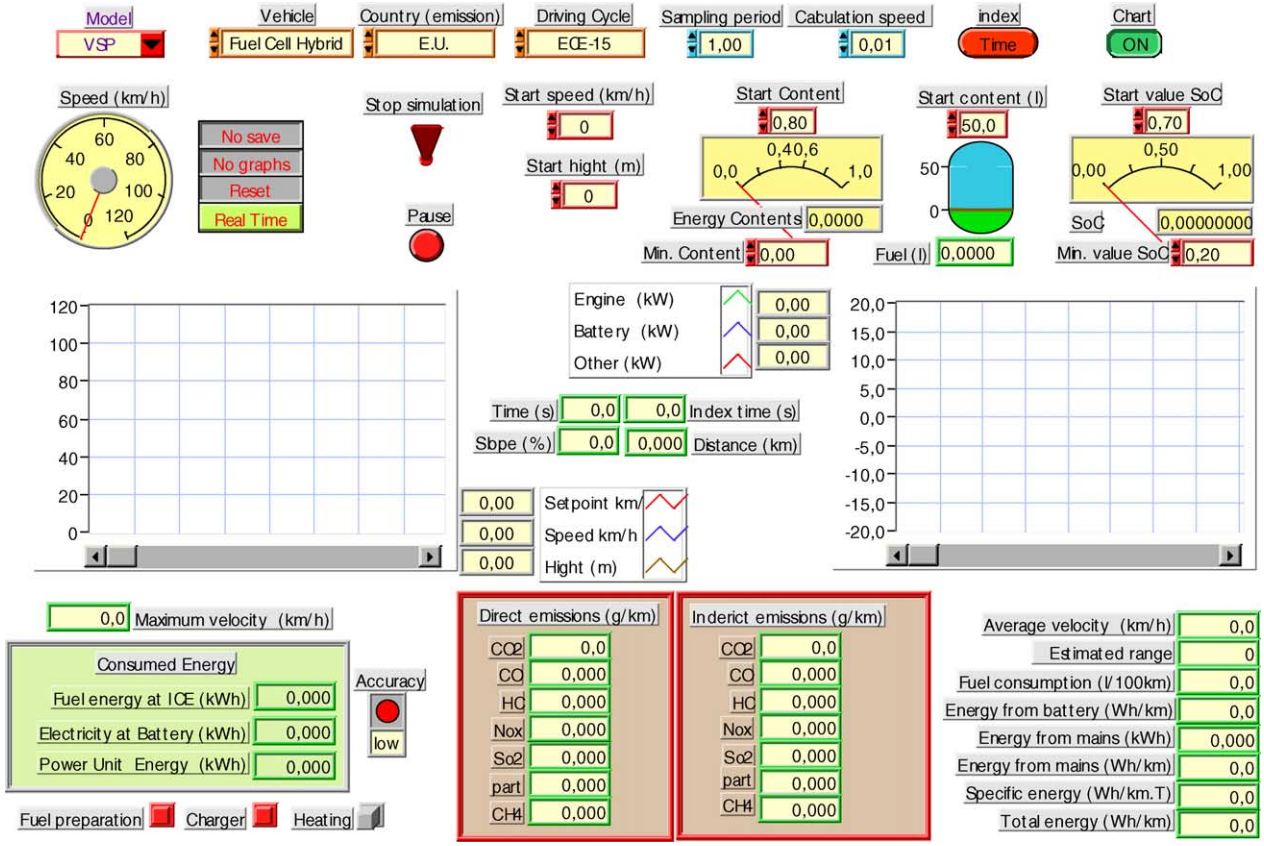

Fig. 2. Vehicle simulation programme.

system producing electric energy starting from stored hydrogen or from a fuel tank feeding a reformer to produce hydrogen [9]. The excess of electricity produced by the fuel cell can be stored in a buffer battery. When the battery is left out one has no longer a hybrid vehicle but a fuel cell electric vehicle. In this case, the fuel cell has to demonstrate enough dynamics to meet variable power demand.

Fig. 1 illustrates a simulation model of a series hybrid with peak power unit, where the generator group provides a constant average power, the battery works as an energy buffer and the flywheel (or ultracapacitor) caters for the brake and acceleration power peaks. In this configuration the battery can be smaller or it can possibly be omitted. The efficiency and reliability of the flywheel or ultracapacitor are an important factor for the development of these drive trains.

This model is part of a vehicle simulation programme (VSP) [2–4] whose front panel is illustrated by Fig. 2 and for which it is necessary to introduce models for all components or subsystems of each simulated vehicle and particularly of the energy and power sources. The basic modelling strategy used in VSP is the well-tried and trusted method of dividing the drive cycle into a number of time steps and calculating the characteristics of the vehicle at the end of each time interval, which is called the longitudinal dynamics simulation [10,11].

This paper will focus on the description of different energy or power sources as well as on their simulation models and calculation results.

2. Fuel cells

2.1. Description of the fuel cell

The fuel cell electrochemically combines the oxygen of air with a hydrogenated fuel and converts them into water and other elements with a production of electricity. The conversion is similar to that of a conventional battery, except that the reductant and oxidant are continuously supplied to the cell instead of being contained in the cell. In addition, fuel cells are 'recharged' by filling up the fuel supply.

When the fuel cell uses hydrogen as a fuel, this hydrogen can either be stored as such in the vehicle, or be generated in the vehicle by means of a reformer. Fuels such as methanol, natural gas, synthesis gas or even conventional hydrocarbon fuels can be used by employing a chemical reactor prior to entering the fuel cell. The fuel is converted into a hydrogen rich synthesis gas via a steam reformer, auto-thermal reformer or a partial oxidising burner. This gas is then purified in a gas purification stage to clean the hydrogen and to scrub CO and CO_2, which are emitted from the process [12].

Hydrogen can be stored as a compressed gas in vessels, as a cryogenic liquid at a temperature of $-253\,^{\circ}C$ or as hydrogen atoms reversibly adsorbed in metal hydrides, which are obtained by applying hydrogen gas under pressure on suitable metal alloys. The low temperature and pressure, at which the reaction occurs and the stability of the hydrides, preventing leakage flows in case of damage, make this form of storage particularly attractive for road transportation applications. Compared to lead acid batteries this storage contains up to 10 times more energy per unit of weight [13].

Fuel cells have the potential to be more efficient than a gasoline or diesel engine. Fuel cells are at the opposite of most electrical devices since peak efficiency occurs at minimum load: efficiency is 60% at no load and 40% at full load at the current state of development, the theoretical maximum being 83% [14]. The fuel cell system has relatively few moving parts (reactant pumps and valves), which produce very little friction. The fuel is oxidised at low temperature instead of being combusted at very high temperatures as in an internal combustion engine. Low emissions are a result of low-temperature oxidation and appropriate fuel selection when a reformer is used with hydrocarbon fuels. If methanol is used to generate hydrogen with a reformer, 25 vol.% of the gas output is CO_2 [15]. In the case of hydrogen (the ideal fuel), the only by-product is water.

Fuel cell systems (e.g. PEMFC) are under development and still relatively large and heavy (also due to the large volume of ancillary equipment) compared to conventional engines. Cost is still very high, mainly because of the use of expensive materials and the low volume production. As manufacturing issues are tackled, lower cost materials should considerably bring the cost down.

The fuel distribution infrastructure for hydrogen is very limited. A reformer based vehicle system has the advantage of using existing hydrocarbon fuels that are more readily available than hydrogen:

- Methanol is a simple molecule, making it relatively easy to reform and it is liquid, so it fits more easily into the existing motor fuel distribution infrastructure. Concerns are raised, however, on its toxicity; the fact that it burns without readily visible flames may also create a potential hazard.
- When using gasoline reformers the existing fuel infrastructure can be used, but their additional emissions are still being examined.
- Hydrogen can also be produced out of natural gas at refuelling stations [16] or by electrolysis of water.

The fuel cell's working principle is very simple, however, the electrochemical reactions do not readily take place, and unless special materials are used for the electrodes and the electrolyte, the current produced per square centimetre is small and the electrical power losses in the electrolyte are large. To overcome these problems, different types of fuel cells have been developed. The different varieties are distinguished by the electrolyte used and have each a particular construction of the electrodes. However, in all types there are separate reactions at the anode and the cathode, and charged ions move through the electrolyte, while electrons move through the external load circuit. Another common feature is that the electrodes should be porous, because

Table 1
Summary of fuel cell types [18]

FC type	Electrolyte	Operating temperature (°C)	Current density	Need for fuel processor	Stage of development	Efficiency prospects	Cost prospects
PEMFC	PEM	70–90	High	Yes	Prototype demonstrated on board of vehicle fleet	Good	Good
AFC	Alkaline	70–100	High	Yes	Space application	Good (70%)	Good
PAFC	Phosphoric acid	200–220	Moderate	Yes	Early commercial (stationary) applications	Good (40%)	Fair
MCFC	Molten carbonate	600–650	High	Yes	Field demonstration, high power applications	Good (60%)	Fair–good
SOFC	Solid oxide	800–1000	Moderate	No	Prototype	Good (60%)	Fair–good
DMFC	PEM	70–90	Moderate	No	Research	Poor (40%)	Poor–fair

the gases have to be in contact with the electrode and the electrolyte at the same time [17]. Table 1 summarises the features of the different fuel cell types.

2.2. Fuel cell model

In the previous section the basic principles of fuel cell are described. However, how can they be expressed in a simulation model? This will be explained hereunder.

The fuel cell model considered is a typical black box approach. This makes it possible to develop in the first instance one simplified model containing the fuel cell stack, the DC–DC convertor, the reformer and the auxiliary system [19].

Up-to-now temperature and pressure effects are not included in the model, due to lack of sufficient data available. A higher stack temperature or lower pressure will lead to a lower voltage level. The start-up process of some fuel cells can be very long and can create considerable additional energy consumption and emissions. The model is based on experimental data of an alkaline fuel cell (AFC), as well as of a proton exchange membrane (PEM) fuel cell [15].

The DC–DC convertor adapts the fuel cell voltage level to the DC-bus voltage or battery voltage. At the moment it is modelled by a simple efficiency value (see (2.1)). The power required for the fuel cell auxiliaries, P_{aux} (pump, compressor, controller) is calculated based on experimental data in function of the required fuel cell power, P_{fc} (see Eq. (2.2)) [15]:

$$P_{fc} = \frac{P_{DC}}{\eta_{conv}} \tag{2.1}$$

$$P_{aux} = a + bP_{fc} + cP_{fc}^2 \tag{2.2}$$

$$P_{ref} = x_{ref} P_{fc} \tag{2.3}$$

$$P_{stack} = P_{fc} + P_{aux} + P_{ref} \tag{2.4}$$

where P_{DC} is the DC/DC convertor power to DC-bus (W); η_{conv} the DC/DC convertor efficiency (%); P_{fc} the fuel cell power (W); a, b, c the constant empirical values; P_{aux} the auxiliary power (W); x_{ref} the reformer coefficient; P_{ref} the reformer power (W) and P_{stack} the fuel cell stack power (W).

The power required for the reformer, P_{ref}, is also taken into account as proportional to the delivered power (Eq. (2.3)). The sum of these power components results in the total required stack power, P_{stack} (Eq. (2.4)). If this stack power exceeds the maximum allowed stack power, P_{max}, the iteration process [20] of the simulation programme will decrease the fuel cell power, P_{fc}.

The fuel cell stack consists of different modules connected in series. Each module is a combination of a number of individual cells in series and different rows of series-cells are connected in parallel. The required power for each cell, P_{cell}, can be calculated by dividing the stack power by the total number of cells. This is an approximation, however, due to the possible unbalance between cells. Based on experimental data the cell current, I_{cell}, can be computed as function of this cell power [15].

In the considered electrical circuit, the fuel cell is mainly characterised by its internal resistance. The dynamic behaviour of the fuel cell has also to be taken into account: the maximum rate of change of the current is dependent on the cell surface. The simulation model shall check the maximum current variation and if necessary it will reduce the required fuel cell power.

The fuel consumption per cell (fcc) is calculated as function of the current law of Faraday, which gives the relation between the reactant consumption and the produced current: 1 g equivalent weight of matter is electrochemically altered at each electrode for 96,489 C of electricity passed through the electrolyte. Two gram of hydrogen (H_2) produces 192,978 Ampere–seconds (A s) or 53.61 Ampere–hours (A h). The elimination (purge) of impurities is taken into account with a correction factor (e.g. 1.012 in Eq. (2.5)) [15]. The fuel consumption corresponds with a certain fuel power content as function of the density, D (kg/m^3), and the specific energy, E_{H_2} (Eq. (2.7)):

$$\text{fcc} = 1.012 \frac{I_{cell}\, 22.4\ (\text{l/mol})}{2.96489\ (\text{A s/mol})} \tag{2.5}$$

$$\text{Cons} = \text{Nr}_{cells}\, \text{fcc} \tag{2.6}$$

$$P_{\text{fuel}} = \text{Cons}\, E_{H_2}\, D \times 10^6 \quad (2.7)$$

where I_{cell} is the cell current (A); fcc the fuel consumption per cell (l/s); Cons the fuel consumption of the whole stack (l/s); Nr_{cells} the number of cells; D the fuel density (kg/m^3); E_{H_2} the specific energy (MJ/kg) and P_{fuel} the fuel power (W).

The emissions are calculated proportional to the fuel consumption [21] of the related reformer. This is a very simplified approach that only gives an indication of the order of magnitude of the emissions. Additional data has to be available for the extension of the model. This model is an unpretentious model, but due to the black box approach it can easily be completed as soon as more experimental data are available, for example, out of the ELEDRIVE thematic network [22].

2.3. Calculation results of the fuel cell model

Fig. 3 illustrates the simulation result of a fuel cell used in a 2.7 t hybrid electric van driving an ECE-15 speed cycle. The input parameters are the requested fuel cell power as well as the composition of the fuel cell stack (number of individual cells). The graphs in Fig. 3 illustrate the voltage, current and power delivered by one cell of the fuel cell stack.

In this example the simulated power management strategy of the hybrid drive train consists in continuously charging the battery at 5 kW, while the fuel cell delivers this charging power as well as the power requested by the electric traction motor for driving. This somewhat exotic power management was selected to better illustrate the dynamics in the power delivered by the fuel cell. Another strategy could consist in delivering constant power by the fuel cell, the battery being in charge of all power dynamics.

3. Battery

3.1. Battery description

Batteries are characterised by their life cycle, energy and power density and energy efficiency. The *life cycle* represents the number of charging and discharging cycles possible before it loses its ability to hold a useful charge (typically when the available capacity drops under 80% of the initial capacity). Life cycle typically depends on the depth of discharge. When charging and discharging a battery not all energy, delivered to the battery, will be available due to battery losses, which are characterised by the *battery efficiency*. The *specific energy* and *power* describe, respectively, the energy content (determining the vehicle range) and the maximum power (determining the vehicle acceleration performance) in function of the weight of the battery. A battery can be optimised to have a high energy content or it can be optimised to have a high power capability. The first optimisation is important for battery electric vehicles, while the second is mainly required for hybrid drive trains. Hybrid drive trains lead also to the consideration of a mixed energy-power capability.

A specific energy of at least 50 W h/kg and a specific power ranging from 100 W/kg, continuous, up to 200 or 300 W/kg intermittent pulse power is a must for an good electric vehicle design. Ideally, 150 W h/kg and/or 500 W/kg up to 1000 W/kg (in the case of super-capacitor) would be better, especially for hybrid vehicles [9]. The US Advanced Battery Consortium (USABC) midterm goals are 150 and 135 W h/kg and long-term goals 400 and 300 W h/kg for, respectively, battery power and energy density.

As is usual in electric circuit theory the maximum power is defined for the system delivered rate current at a terminal voltage that equals 50% the initial open circuit voltage [23].

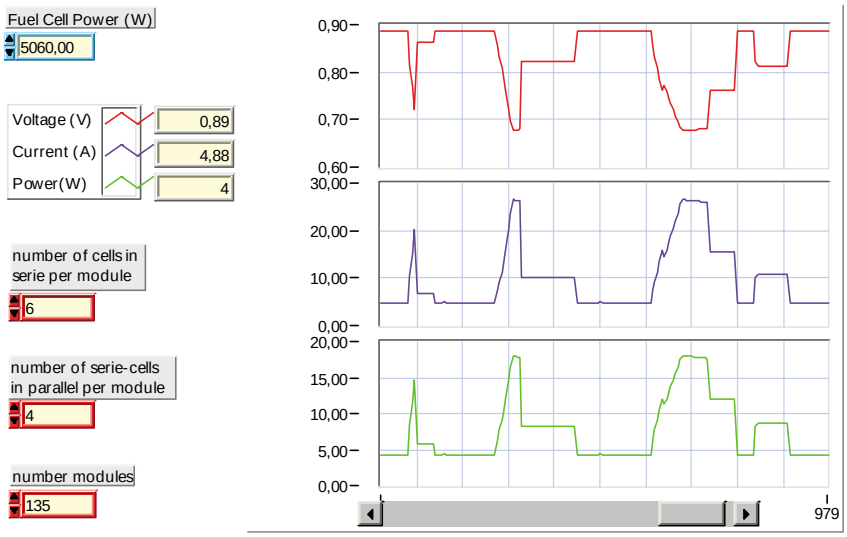

Fig. 3. Simulation result of a fuel cell model.

In the IEC standard [24] the maximum deliverable battery power is defined as the power corresponding to rated current and the battery terminal voltage would fall at 2/3 of the open circuit voltage.

A battery for an electric vehicle consists of a combination in series, and possibly parallel, of individual battery cells. Minor differences in cell characteristics can be present. Consequently, a battery management system controlling the state of each cell is a key point for battery reliability and life duration.

3.2. Battery model

The model described is the one of a lead acid battery. Similar models for other batteries are possible. The model tracks the state of charge (SoC) according to the current drawn from the battery. The SoC is the relative remaining capacity, C_I, of the battery, expressed in %. Discharging during a period T_s with a current I_{bat} leads to a SoC equalling:

$$\mathrm{SoC} = 1 - \frac{I_{bat} T_s}{C_I\, 3600} \tag{3.1}$$

The C_5-capacity is the number of Ampere–hours (A h), which can be drawn out of the battery during 5 h with a current equal to C_5 divided by 5 (i.e. one-fifth of the rated Ampere–hours in 5 h discharge).

The effect of ambient temperature, t_a^0 (in °C) on the capacity is taken into account with the help of an empirical formula. An example for a lead acid battery is give by Eq. (3.2) [25]. The influence of age, number of discharge/charge cycles are yet not taken into account. The C_5-capacity has to be multiplied by the number of series-cells in parallel, $\mathrm{Nr^p}$, to get the total battery capacity, C_{tot}:

$$C_{tot} = \frac{\mathrm{Nr^p} C_5}{1 + 0.006(30 - t_a^0)} \tag{3.2}$$

Within this model a subprogramme characterising the cell-module is used to calculate the open circuit voltage of the battery pack, U_0, and the internal resistance, R_i, both dependent on the current SoC, the temperature and on discharge or charge condition (Eqs. (3.3) and (3.4)). The dependence of the internal resistance of a lead acid battery on the SoC, for example, is due to the variation of electrolyte conductivity and of the bad conducting lead sulphate which deposed on the electrodes during discharge. The dependency on the internal resistance on the SoC is bound to the battery type. These figures can be measured for charging as well as for discharging. Notice that the model does not take into account the possible unbalance between cells or monoblocs.

$$U_0 = \mathrm{Nr^s}\, f(\mathrm{SoC}, t^0) \tag{3.3}$$

$$R_i = \frac{\mathrm{Nr^s}}{\mathrm{Nr^p}} f(\mathrm{SoC}, t^0) \tag{3.4}$$

where $\mathrm{Nr^s}$ is the number of cells in series; $\mathrm{Nr^p}$ the number of series-cells in parallel; t^0 the cell temperature (°C); U_0 the open-loop voltage (V) and R_i the internal resistance (Ω).

The available capacity of the battery changes as function of the discharge (or charge) current. The implemented model tracks the SoC according to the current drawn from the battery. On the bases of the actual battery current I_{bat} and the time increment T_s, the variation of SoC, ΔSoC is calculated. It is primarily based on the empirical law of Peukert [26,27].

Peukert's equation is a formula that shows how the available capacity of a battery changes according to the rate of discharge. The capacity of a battery is expressed in Ampere–hours (A h), but it turns out that the simple formula of current times hours does not accurately represent the situation. Peukert found that Eq. (3.5) fits better the observed behaviour of batteries:

$$C = I^{\mathrm{k}}\, \mathrm{Time} \tag{3.5}$$

The equation captures the fact that at higher currents, there is less available energy in the battery. C is the theoretical capacity of the battery and I the current, Time the total charge time, and k the Peukert number, a constant for a given battery. A value close to 1 indicates that the battery performs well. The higher k, the more capacity is lost when the battery is discharged at high currents. The Peukert number of a battery is determined empirically and lies normally between 1.2 and 1.4 for lead acid batteries. If k would be selected equal to 1, a linear relation between SoC and capacity would be assumed, as this is practically the case for $NaNiCl_2$ batteries. Fig. 4 represents this equation for different values of k. It is quite remarkable that discharging at 0.1 times the nominal current increases the capacity with a factor 2 when the battery has a Peukert constant k equals 1.3.

When the 5-h rate capacity, C_5, is given the Peukert expression can be used to calculate the capacity for any given current:

$$C_I = C_5 \left(\frac{I_5}{I_{bat}} \right)^{k-1} \tag{3.6}$$

The substitution of (3.6) in (3.1) gives:

$$\mathrm{SoC} = 1 - \frac{I_{bat} T_s}{C_5\, 3600} \left(\frac{I_{bat}}{I_5} \right)^{k-1} \tag{3.7}$$

This law is transformed into (3.8), which expresses the SoC increment, ΔSoC. This equation assumes that the current I_{bat} remains constant during one step T_s of the simulated speed cycle. In this equation, C_{tot} (Eq. (3.2)), taking into account the temperature effect, replaces C_5:

$$\Delta\mathrm{SoC} = \frac{T_s}{3600} \frac{|I_{bat}|^k}{(C_{tot}/5)^{k-1} C_{tot}} \tag{3.8}$$

To be able to implement this formula the knowledge of the battery current is required. This value can be calculated based on the fundamental electric equations (3.9) and (3.10), which describe the simple battery model of Fig. 5. Transforming these formulas gives (3.11), which defines the battery current I_{bat} as function of the required battery power P_{bat}, the internal resistance R_i and the open-loop voltage U_0:

$$U_{bat} = U_0 - R_i I_{bat} \tag{3.9}$$

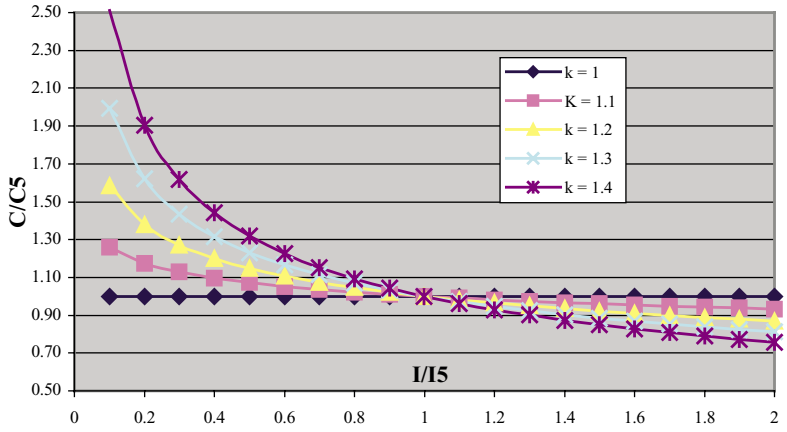

Fig. 4. The battery capacity vs. discharge current.

$$P_{\text{bat}} = U_{\text{bat}} I_{\text{bat}} \tag{3.10}$$

$$I_{\text{bat}} = \frac{U_0 - \sqrt{U_0^2 - 4P_{\text{bat}}R_{\text{i}}}}{2R_{\text{i}}} \tag{3.11}$$

Dynamic modelling of a battery is extremely difficult. Understanding what is going on in batteries requires several years of thorough research effort. Finding the right equation to describe these phenomena is not straightforward, especially when they have to be implemented in a simulation tool. The time constant characterising the dynamic behaviour of the battery (e.g. the battery voltage) is of the same order of magnitude as the mechanical driving time constants. A dynamic battery model can thus lead to a more accurate simulation result. Different models have already been proposed. Fig. 6 illustrates an example of a dynamic battery model for a lead acid battery [28]. Fig. 7 shows a possible equivalent circuit for a NiCd battery [29]. Specific battery management and test infrastructure has recently been developed at the Vrije Universiteit Brussel to perform dynamic battery testing in a well-controlled environment. With the help of powerful surface fitting algorithms, dynamic models as well as a new type of SoC-indicator are under development. Up-to-now a maximum open-loop voltage deviation in time is implemented in the software model.

With some types of batteries the electrolyte can start gassing when the battery cell voltage exceeds a certain level, U_{g}, and the charge acceptance goes down. For lead acid batteries gassing occurs above 2.4 V per cell. Whenever the voltage exceeds this value a constant charge acceptance of 80% is assumed in the simulation.

In Eq. (3.11) a square root is taken. If the argument of this square root is negative, it means that the battery is not able to deliver the required power, P_{bat}. The maximum power that can be delivered is thus given by Eq. (3.12). Remark that according to Eq. (3.11) the battery is able to accept negative powers of any amplitude since the square root then certainly is a real value:

$$P_{\text{max}} = \frac{U_0^2}{4R_{\text{i}}} \tag{3.12}$$

When the battery cell voltage exceeds the maximum allowed voltage, $U_{\text{max}}^{\text{cell}}$ (e.g. during regenerative braking on a fully charged battery), the battery power is limited to the corresponding maximum power, $P_{\text{max}}(U_{\text{max}})$ (Eq. (3.13)). And vice versa, when the battery cell voltage drops under a minimum level, $U_{\text{min}}^{\text{cell}}$ (e.g. during strong acceleration) the corresponding maximum power, $P_{\text{max}}(U_{\text{min}})$, is calculated with Eq. (3.14). Note that $P_{\text{max}}(U_{\text{max}})$ is always positive and $P_{\text{max}}(U_{\text{min}})$ always negative. The possible battery power,

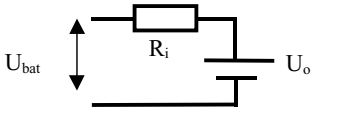

Fig. 5. Equivalent scheme of a simple battery model.

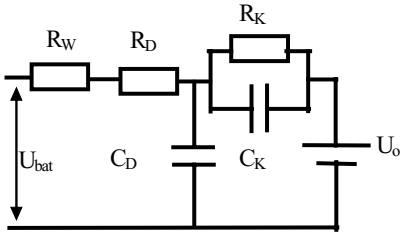

Fig. 6. Dynamic battery model.

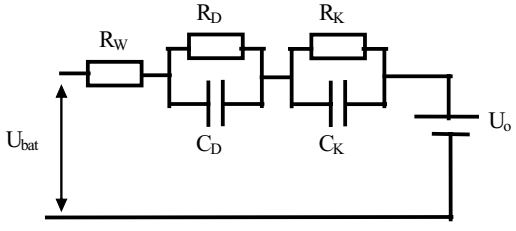

Fig. 7. Equivalent circuit for the NiCd battery.

Table 2
Speed cycle: simulation vs. measurements

	Measured	Simulation	ECE-15
Ah discharged	1.52	1.46	1.53
Ah charged	0.19	0.18	0.19
Total Ah	1.33	1.28	1.34
Recuperation (%)	12.35	12.20	12.71

P_{pos}, is thus limited to one of these values (Eq. (3.15)). These voltage limits U_{max} and U_{min} are required in real life too. Outside these limits irreversible electrochemical process will damage the battery:

$$P_{max}(U_{max}) = \frac{U_0 - Nr^s U_{cell}^{max}}{R_i} Nr^s U_{cell}^{max} \quad (3.13)$$

$$P_{max}(U_{min}) = \frac{U_0 - Nr^s U_{cell}^{min}}{R_i} Nr^s U_{cell}^{min} \quad (3.14)$$

$$P_{pos} = P_{max}(U_{max}) \vee P_{max}(U_{min}) \quad (3.15)$$

Furthermore two other operating limits are implemented in the simulation programme: the maximum battery charge current, I_{max}^{ch}, and the maximum discharge current, I_{max}^{dis}.

3.3. Calculation results of the battery model

To illustrate the battery model some simulations as well as on-road measurements were performed for a passenger car equipped with a DC separated excited motor and a NiCd battery. The same speed cycle as the one driven on road is simulated. The comparison of both simulated and measured parameters demonstrates a good correlation (see Table 2). The relative error is less than 5%.

One of the most difficult experiments to simulate, while the battery model plays an important role, is an acceleration test. Contrary to a comparison based on a pre-defined speed cycle, one is not performing a straightforward step-by-step calculation, but for each point the simulation has to iterate towards the possible working point [1]. A little error in the beginning can, due to integration, result in a large deviation at the end of the simulation.

In Fig. 8 one can find the measured speed compared against the simulation results when the acceleration of the vehicle is at its maximum. The boundaries of the motor are the maximum speed and torque. This motor was current controlled. A current limit (as a function of the revolutions per minute) is introduced too. Simulated values are marked with 's' and measured values with 'm'. The good correlation between the measurement and the simulation demonstrates the performance of the iteration algorithm. An average deviation of 2% is found.

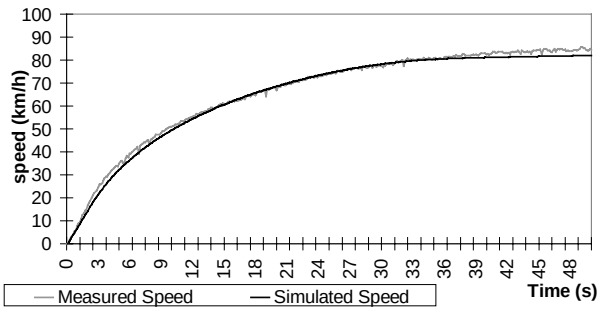

Fig. 8. Acceleration simulation vs. measurement.

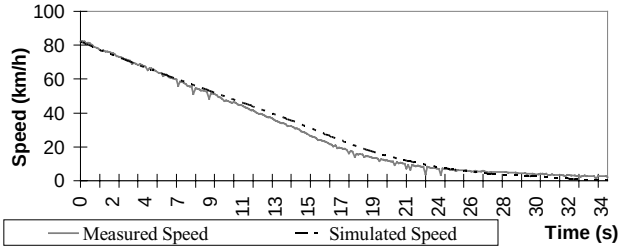

Fig. 9. Deceleration simulation vs. measurement.

In Fig. 9 one can see the deceleration test. During this test only regenerative braking by the motor was performed, without using any mechanical brakes. The graph of Fig. 10 compares the DC motor current (Imot) and DC voltage (Umot) for the acceleration and deceleration test. The little deviation in current can be explained by a possible minor frontal or back wind and by a road inclination during the on-road measurement. The graph of Fig. 11 shows, for the same acceleration test, the variations in current (Ibat) and voltage (Ubat) of the battery.

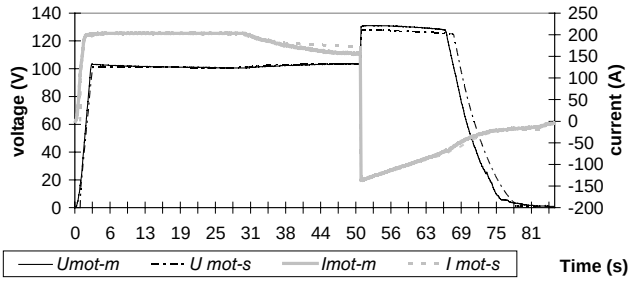

Fig. 10. DC motor current and voltage comparison.

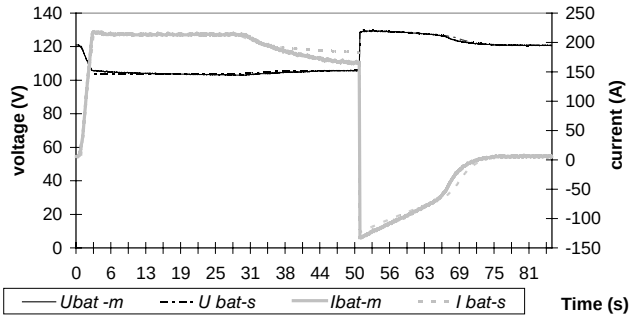

Fig. 11. Battery voltage and current.

4. Ultracapacitor

4.1. Ultracapacitor description

Super or ultracapacitors (800–1500 F) behave, like very high-power, low-capacity batteries but store electric energy by accumulating and separating opposite charges physically, as opposed to batteries, which store energy chemically in reversible chemical reactions. One key aspect of super-capacitors is that they demonstrate excellent life cycle. When fully developed for vehicles, they could be expected to last as long as the car. This is because it is possible to cycle ultracapacitors very quickly without having the large decrease in life cycle that most chemical batteries experience. They also have a high cycle efficiency (up to 90% [30]) compared with chemical batteries. The primary obstacles with ultracapacitors at this time are their low specific energy, which are in the range 5–10 W h/kg and the large possible voltage dispersion between individual cells. Ultracapacitors also have the unique feature that their voltage is directly proportional to their state-of-charge. Therefore, either their operating range must be limited to high state-of-charge regions, or control electronics must be used to compensate for the widely varying voltage. A voltage drop of 50% can be allowed, which corresponds to 75% of the energy content. The fact that super-capacitors can provide high power for accelerations and can accept high power during regenerative braking makes them ideally suited for the load levelling required in electric and hybrid electric vehicle. Power densities of 2000–4000 W/kg have been demonstrated by ultracapacitors in the laboratory [31].

4.2. Ultracapacitor model

The model of an ultracapacitor can be developed in a similar way as that of the battery. The voltage, U_c, over the capacity, C, has the same roll as the open-loop voltage, U_0, of the battery. The capacity voltage, U_c, changes with the electrical charge, q. The electrical charge will change in function of the cell current, I_{cell}, [32]:

$$U_c = \frac{q}{C} \tag{4.1}$$

$$q_{t+1} = q_t - I_{cell} T_s \tag{4.2}$$

The equivalent circuit (Fig. 12) is also similar to the battery model.

Several capacitors can be connected in series, Nr^s, and in parallel, Nr^p. This result in the total capacity voltage, U_{cap}, and current, I_{cap} (Eqs. (4.3) and (4.4)). The internal resistance, R_i, is dependent on the current and temperature [33]:

$$U_{cap} = Nr^s (U_c - R_i I_{cell}) \tag{4.3}$$

$$I_{cap} = Nr^p I_{cell} \tag{4.4}$$

Additionally, the self-discharge of the capacitor should be taken into account with the resistance, R_p [30]. This model does not take into account the possible unbalance between individual cells. This model can be used as a black box model that is connected to the propulsion system via a DC/DC converter.

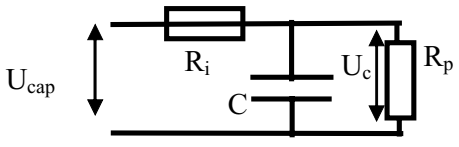

Fig. 12. Ultracapacitor equivalent circuit.

5. Flywheel

5.1. Flywheel description

Flywheels store energy mechanically in the form of kinetic energy. One can distinguish mechanical and electrical flywheels. The mechanical flywheel is connected to the drive system via an axle. The electrical flywheel takes an electrical input to accelerate its rotor by using a built-in motor, and returns the energy by using this same motor as a generator.

The most significant factor affecting flywheel design is the material used to construct the flywheel rim. A flywheel rim needs to be made of a high tensile strength to density ratio material to maximise the kinetic energy stored (thanks to a high rotational speed) while minimising the chance of failure. Flywheels show technical promise as a potential load-levelling device for hybrid electric vehicles; however, they are still under development. Flywheels could become an excellent high power density storage devices. An optimistic estimate for specific power is ranging between 2000 W/kg (short-term) and 8000 W/kg (long-term) [34]. The corresponding specific energy is ranging from 4 to 50 W h/kg [35].

5.2. Flywheel model

The required flywheel-convertor power, P_{req}, will be divided by the convertor efficiency, η, including convertor losses and all flywheel losses except the friction moment. This required power is compared with the maximum power, P_{max}, that the flywheel can deliver. The flywheel current rotational velocity, ω_{fw}, the maximum acceleration, a_{max}, the flywheel inertia, J, and the maximum torque, T_{max}, define this maximum power:

$$P_{max} = \omega_{fw} \max(T_{max}, J a_{max}) \tag{5.1}$$

The flywheel velocity must be kept above a certain minimum speed, ω_{min}, otherwise the flywheel will not be able to deliver power and below a maximum velocity, ω_{max}, to avoid mechanical damage.

The maximum velocity defines the maximum energy content of the flywheel, E_{max} (Eq. (5.2) which corresponds with a SoE equal to 1). To avoid confusion with the battery model, a state of energy is used in the flywheel model instead of a SoC. Up to 80% of this energy can be used during operation of the flywheel:

$$E_{max} = \frac{\omega_{max}^2 J}{2.3600} \tag{5.2}$$

Even if the flywheel is not delivering power, its energy content, E_{cons}, will decrease due to the friction moment, T_{fr}. The energy consumption, E_{cons}, is computed as function of the simulation time increment, T_s, using the following equation:

$$E_{cons} = \frac{T_s}{3600}\left(T_{fr}\omega_{fw} + \frac{P_{fw}}{\eta}\right) \tag{5.3}$$

The flywheel energy will decrease or increase as function of the sign of the flywheel power, P_{fw} (Eq. (5.4)):

$$E_{fw}^t = E_{fw}^{t-1} - E_{cons} \tag{5.4}$$

The corresponding flywheel state of energy and angular velocity can be calculated according to the following equations:

$$\text{SoE} = \frac{E_{fw}^t}{E_{max}} \tag{5.5}$$

$$\omega_{fw} = \sqrt{\frac{E_{fw}^t\, 3600.2}{J}} \tag{5.6}$$

where E_{fw}^t is the flywheel energy at instant t (W h); E_{fw}^{t-1} the previous flywheel energy at instant t (W h); ω_{fw} the velocity (rad/s) and J the inertia (kg m^2).

5.3. Calculation results of the flywheel model

Fig. 13 shows the simulation results of an electric drive with a flywheel as energy source delivering the traction power for driving an ECE-15 speed cycle. At the end of the cycle the flywheel is recharged with a constant power of 2500 W. On the left side of Fig. 13 one can find settings indicating the required power as well as some constant model parameters like maximum and minimum flywheel speed and its maximum deliverable torque. The graph in the middle of Fig. 13 illustrates the flywheel speed, torque and power. The flywheel speed changes in function of the delivered power.

On the right side of Fig. 13 some other constant parameters, like weight, friction moment, converter efficiency, flywheel inertia and maximum acceleration, can be found. Finally, on the left side the output parameters can be found, namely the delivered power (inclusive losses), rotational speed, efficiency and SoC as well as the maximum available power.

6. Engine-generator group or APU

6.1. Engine

The engine model described in this chapter can be used in a classical thermal vehicle as main motor or in a hybrid vehicle as part of the APU. It is mainly based on look-up tables of engine maps and calculates the emissions and fuel consumption.

The total engine torque, T_{ice}, is function of engine inertia, J, vehicle acceleration, T_a, resistive torque, T_r, and auxiliary alternator power, P_{alt}, as shown by the following equation:

$$T_{ice} = T_r + \frac{P_{alt}}{\omega_{ice}} + T_a + Ja \tag{6.1}$$

Internal combustion engines require a minimum shaft speed, below which they will stall. This is implemented in the clutch or in the control algorithm of the hybrid vehicle.

Fig. 13. Simulation result of a fuel cell model.

If the engine is running, with the engine velocity higher than idle speed and the resistive torque different from zero, then the engine is in normal operating mode (see further down). If not, the engine can be in off-mode with the 'key switch' and all output parameters at zero. If the key switch is on, with the engine velocity strictly lower than idle speed, then the engine is starting.

The user can select a start-up penalty. This start-up penalty has to be measured and can be imported as a cluster of correction factors for each type of emission and for the fuel consumption. This can be done for different engine start-up temperatures. Hence the additional fuel consumption and emissions can be taken into account at start-up. If the user prefers not to use this feature or the data is not available, the idle emissions and consumption are used during this start-up phase.

In normal operating mode the maximum torque is defined in a look-up table as function of the angular velocity and the total torque. Once the possible engine torque is known the emissions (in g/s) and fuel consumption (in l/s) can be calculated on the basis of iso-emission and consumption curves (in g/kW h). Out of the possible speed and torque values, the emissions are calculated using bilinear interpolation of the discretised iso-emission curves, which are entered in several arrays. These curves or maps describe the static behaviour of an internal combustion engine. This works when transients are negligible. However, if transients are large the interpolated results may be wrong with several orders of magnitude [36].

If the engine torque is negative—the engine is slightly braking the drive train—a small (lower than idle mode) constant value or zero fuel consumption and emission is assumed.

The engine will produce additional emissions when the engine is cold. A cold/hot emission ratio can be introduced, which is a function of ambient temperature and trip length [37–39]. The user can select if the motor operates in a warm mode or cold mode. In the case of a cold engine an additional penalty is implemented based on an empirical model, which describes emissions and fuel consumption correction factor as function of the ambient temperature and fuel type [37].

The mechanical power, P_{ice}, at the engine shaft (Eq. (6.2)) as well as the power of the consumed fuel, P_{fuel} (Eq. (6.5)) is calculated. The last one is a function of the fuel density, D, and fuel specific energy, E_{fuel}:

$$P_{ice} = \omega_{ice} T_{ice} \tag{6.2}$$

$$\text{fco} = \text{fco}(\omega_{ice}, T_{ice}, t_a^0) \tag{6.3}$$

$$\text{Cons} = \frac{\text{fco}}{1000\, D} \tag{6.4}$$

$$P_{fuel} = \text{Cons}\, E_{fuel} \times 10^6 \tag{6.5}$$

where T_{ice} is the total engine torque (N m); T_r the resistive torque (N m); P_{alt} the alternator power (W); T_a the acceleration torque (N m); ω_{ice} the angular velocity (rad/s); P_{ice} the mechanical shaft power (W); t_a^0 the ambient temperature (°C); fco the fuel consumption (g/s); D the fuel density (kg/l); Cons the fuel consumption (l/s); E_{fuel} the specific energy (MJ/l) and P_{fuel} the fuel power (W).

If engine data corresponding to an engine with a certain required size is not available, an engine can be selected out of the database and its characteristics can be scaled down (or up) by the help of a scaling factor as a first approximation.

Notwithstanding that the engine model considers cold operation and start-up penalties, it is still a rather simple model. Several other parameters, not taken into account up-to-now, can influence the fuel consumption and emissions.

The model does not consider any time delay associated with fuel transport or torque production. The model does not simulate cranking or associated emissions. No transients of any kind are included. Mean value torque model is used, corresponding to the average torque over the engine cycle.

Recent investigations carried out in the frame of the German and Swiss emission factor programme have shown that it is necessary to take into account the influence of altitude when determining pollutant emissions for the vehicle concepts investigated in cases where a major proportion of the mileage is on roads at a high elevation [39].

In the case of conventional spark-ignition and diesel vehicles, the emission behaviour generally deteriorates within a service interval. In the case of catalyst vehicles an unavoidable deterioration in the degree of conversion by the catalyst (due to thermal ageing and contamination) leads to an increase in emission with increasing mileage. Defects, tuning errors and lack of maintenance are superimposed, in practical operation, on the physically determined reduction in the degree of conversion by the catalyst. Consequently, the implemented look-up tables describe the engine behaviour corresponding to the age of the characterised engine.

Hydrocarbon emissions from motor vehicles are caused by two major sources: exhaust emissions and evaporative losses through the vehicle's fuel system (storage tank, carburettor or injection system, fuel pipes). Evaporative emissions occur as a result of fuel volatility combined with the variation of the ambient temperature during a 24-h period or the temperature changes of the vehicle's fuel system that occur over a normal driving procedure.

The model could be further improved by taking into account certain high-emission events. Such high-emission events occur during phases of extreme high acceleration and during gear changes. The duration of such an event is usually only a few seconds, but the emissions level might reach many (even up to 20,000) times the level of emissions during normal operation. This is especially true for modern gasoline engines with closed-loop catalytic converters [33].

6.2. Generator

The purpose of the generator model is to start the engine and to control the velocity of the engine as function of a certain optimisation criteria in a series hybrid electric

propulsion system. The input parameter of the generator is the required DC power that it has to deliver to the DC-bus. If one would use an AC-generator the same black box approach is possible, where the generator and the required rectifier are gathered in one model. The generator model differentiates three operating modes: OFF, starting and normal operating.

The generator model will switch the engine *OFF* when this is required by the basic power control algorithm. This can only be done when the starting process is completely finished and when the user did not select to use idle mode (instead of shutting down the engine).

Once the engine is switched off and needs to restart again or if it was never before engaged, it will first pass the *start-up phase* before it can deliver the required power. The corresponding starting will take a certain time, selectable by the user. This starting time, T_{start}, will define a required acceleration, a_{start}, as function of the generator initial speed, ω_{ini}, and the required start-up velocity, ω_{start} (Eq. (6.6)):

$$a_{start} = \frac{\omega_{start} - \omega_{ini}}{T_{start}} \tag{6.6}$$

The generator velocity will increase proportional to this acceleration as function of the simulation time increment (Eq. (6.7)):

$$\omega_{gen}^{t} = a_{start} T_s + \omega_{gen}^{t-1} \tag{6.7}$$

Hence the generator velocity is defined and the resistive output torque, T_r, can be calculated as function of the required generator DC power, P_{DC} (Eq. (6.8)):

$$T_r = \frac{P_{DC}}{\eta \omega_{gen}^{t}} \tag{6.8}$$

where ω_{gen}^{t} is the generator velocity (rad/s); ω_{gen}^{t-1} the previous generator velocity (rad/s); η the generator converter efficiency (%) and T_s the time increment (s).

Due to its inertia, J, accelerating the generator will introduce an additional inertia torque, T_a (Eq. (6.9)). Probably the engine will not be able to deliver this torque, due to the fact its velocity is, e.g. lower than idle speed. At this moment the battery will deliver the inertia power during start-up:

$$T_a = Ja \tag{6.9}$$

Once the generator velocity is higher than the start-up velocity and the generator is not switched off, the *normal operating* mode will be active. In this mode the DC power will be limited to the maximum generator power, P_{max}. The model will also impose a maximum power variation, dP/dt. In this way it is possible to simulate moderate variations of the engine required power. Consequently, the additional fuel consumption due to the dynamic operation of the engine is prevented. Similar to the power variation limitation, the model will impose a given maximum velocity variation or generator acceleration, α_{max}. Hence the additional inertia torque, T_a, due to too fast acceleration, can be limited.

In the series hybrid vehicle, the engine velocity is independent from the vehicle velocity. This makes it possible to control the generator speed in such a way to operate the engine following different criteria like:

- At constant speed independent from the required power;
- At a velocity corresponding to the minimum fuel consumption of the engine as a function of the required generator power;
- At a velocity corresponding to the minimum NO_x emissions (or other pollutant) of the engine as function of the required generator power;
- At a velocity corresponding to a rule that is a compromise between fuel consumption and emission minimisation of different pollutants. An energy optimisation does not automatically imply optimisation of the emissions.

These criteria can be implemented with the help of a look-up table that describes the relation between generator power and generator velocity.

The efficiency can be defined with the help of statistical surface fitting models based on measured data as function of, e.g. the generator power and velocity. Comparable to the start-up mode the resistive torque T_r is calculated using Eq. (6.8).

The generator mechanical power is calculated using the following equation:

$$P_{gen} = (T_r + T_a)\omega_{gen} \tag{6.10}$$

6.3. Calculation results of the generator engine model

For the illustration of the generator-engine model the following assumptions are made:

- The vehicle is driving the ECE cycle.
- The APU consists of a generator connected to a diesel engine.
- The maximum acceleration of the generator is set to 4 rad/s^2.
- The maximum APU-power deviation is set to 10 kW/s.

Fig. 14 represents an example of a series hybrid electric vehicle (SHEV) in which the APU delivers a constant power of 24 kW to the DC-bus. This power corresponds to the highest fuel efficiency.

The battery is recharged with a power corresponding to the APU power minus the required driving power. During braking, the brake power will charge the battery too (see green line). After 90 s the battery power reaches its maximum allowed value (see Fig. 14). The iteration algorithm of the software tool will reduce as function of the power management strategy, the APU power, to keep the battery power within limits.

In the beginning of the speed cycle (first 3 s) the engine start-up process can be noticed. A look of this process is illustrated with Fig. 15.

Before the APU can deliver power the engine velocity is brought above idle speed (first 4 s). The battery delivers the required power (battery power (green line) is positive) via

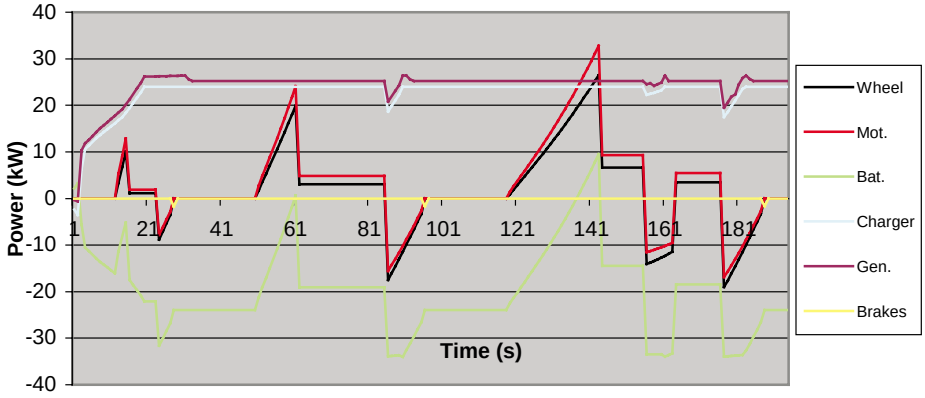

Fig. 14. SHEV-ECE-maximum regeneration power.

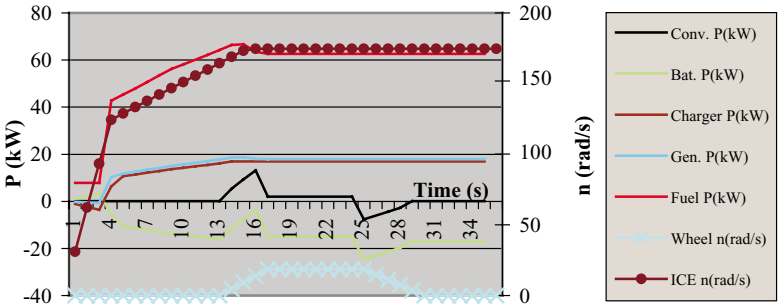

Fig. 15. SHEV-engine start.

the charger (this is the converter connected to the generator). This power corresponds to the model with the inertia of the APU. The start-up acceleration is defined by the start-up time and the required idle speed. Once the engine velocity exceeds the idle speed, the engine will further accelerate to the required operating setpoint. The generator control process defines this acceleration. After 17 s the APU delivers a constant power.

7. Conclusions

Since years ago the automotive industry and several research institutes have developed simulation models to evaluate vehicle performance, fuel consumption and emissions. Most models are oriented towards conventional vehicles with internal combustion engines.

The VSP developed by the Vrije Universiteit Brussel also allows the simulation of these drive trains, however, it is especially develop to simulate battery, hybrid and fuel cell electric vehicles. A great attention is devoted to the modularity of the simulation models, especially the different energy sources used in these electric drive trains. The software tool has a flexible database structure, integrated in the component models, allowing an easy implementation of different kind of component description, in the form of look-up table, maps, theoretical equations, and empirical formula, in function of the available data.

This paper gives an overview of different energy sources applicable in electric and hybrid vehicles. Simulation models for fuel cells, batteries, ultracapacitors, flywheels and engine-generator units were described. These components were described in three stages: first their functionality and characteristics are described; next the way these characteristics can be implemented in a simulation model is discussed and finally these principles are illustrated with the help of some calculation results.

Because of nontrivial difficulties to access data, the models are a trade-off between complex detailed accurate models and models based on easy-available data. Nevertheless, the use of detailed data is possible. The simulation results illustrate the ability of the VSP. The models of the different energy sources are developed in such a way that they are easily interchangeable and hence allowing a flexible evaluation of different drive train structures and their internal power flows.

A good correlation between measurements and simulation results is found, which demonstrates the high simulation accuracy.

Up to now the software was especially develop for the evaluation of electric vehicles as well as hybrid drive trains and their complex power managements strategies. Further

work is being done to extend the component database as well as to further validate the software and this especially in the field of state of the art fuel cell systems.

References

[1] J. Van Mierlo Simulation software for comparison and design of electric, hybrid electric and internal combustion vehicles with respect to energy, emissions and performances, Ph.D. Thesis, Department Electrical Engineering, Vrije Universiteit Brussel, Belgium, April 2000.

[2] J. Van Mierlo, G. Maggetto, Vehicle simulation program: a tool to evaluate hybrid power management strategies based on an innovative iteration algorithm, J. Automot. Eng., SAE IEE 215 (9) (2001) 1043L–1052L.

[3] J. Van Mierlo, G. Maggetto, Views on hybrid drive train power management strategies, in: Proceedings of the EVS-17, Montreal, Canada, October 2000.

[4] J. Van Mierlo, G. Maggetto, Innovative iteration algorithm for a vehicle simulation programme, IEEE Trans. Veh. Technol., submitted for publication. ISNN 0018-9545.

[5] J. Van Mierlo, G. Maggetto, E. Van De Burgwal, R. Gense, Driving style and traffic measures influence vehicle emissions and fuel consumption, in: Proceedings of the Institution of Mechanical Engineers, Part D, J. Automob. Eng., I MECH E, SAE and IEE (2003). ISNN 0954-4070.

[6] J. Van Mierlo, G. Maggetto, et. al., Comparison of the environmental damage caused by vehicles with different alternative fuels and drive trains in a Brussels context, in: Proceedings of the Institution of Mechanical Engineers, Part D, J. Automob. Eng., I MECH E, SAE and IEE 217 (D7) (2003). ISNN 0954-4070.

[7] J. Beretta, New classification on electric-thermal hybrid vehicles, in: Proceedings of the EVS-15, Brussels, Belgium, October 1–3, 1998.

[8] J. Van Mierlo, B.K. Bimbi, G. Maggetto, Comparison of power control algorithms in hybrid vehicles, in: Proceedings of the EVS-15, Brussels, Belgium, October 1998.

[9] G. Maggetto, H. Kahlen, Electric and hybrid vehicles, in: Proceedings of the EPE-97, Norwegian University of Science and Technology, Norway, 1997.

[10] T. Markel, et al., Advisor: a systems analysis tool for advanced vehicle modeling, J. Power Sour. 110 (2) (2002) 255–266.

[11] K.B. Wipke, et al., Advisor 2.1: a user-friendly advanced power train simulation using a combined backward/forward approach, IEEE Trans. Veh. Technol. 48 (6) (1999) 1751–1761.

[12] R. Wurster, PEM fuel cells in stationary and mobile applications: infrastructure requirements, environmental benefits, efficiency advantages and economical implications, Ludwig-Bölkow-Systemtechnik GmbH, Ottobrunn, Germany. http://www.hydrogen.org/.

[13] H. Vandenborre, Technical and economical comparison between a conventional trolley bus system and a bus system based on electrolytic hydrogen, AVERE contract P-016 of the EDS study, Advanced electric drive systems for buses, vans and passenger cars to reduce pollution (EDS), AVERE, Brussels, Belgium, December 1992.

[14] R.L. Hodkinson, Advanced fuel cell control system, in: Proceedings of the EVS-15, AVERE, Brussels, Belgium, October 1998.

[15] H. Van den Broeck, G. Maggetto, Fuel cells and reformers, AVERE contract P-001 of the EDS study, Advanced electric drive systems for buses, vans and passenger cars to reduce pollution (EDS), AVERE, Brussels, Belgium, December 1992.

[16] K. Dircks, Recent advances in fuel cells for transportation application, in: Proceedings of the EVS-15, AVERE, Brussels, Belgium, October 1998.

[17] M. Juhala, P. Sainio, M. Melin, Fuel cell technology: state-of-the-art, in: Proceedings of the Nordisk Miljöbil'99, Helsinki, Finland, September 8–9, 1999.

[18] G. Budd, Fuel cell advances and challenges faced in their implementation within the transportation industry, in: Proceedings of the EVS-17, Montreal, Canada, October 2000.

[19] A. Vannerum, Studie van de Nieuwste Technologische Ontwikkelingen Bij Elektrische Voertuigen (Brandstofcellen, Vliegwielen, Supercondensatoren) A.D.H.V. Simulatiemodellen, Thesis, Vrije Universiteit Brussel, Belgium, pp. 94–95.

[20] J. Van Mierlo, G. Maggetto, Simulation of a complex parallel-series hybrid drive train, in: Proceedings of the EVS-16, Beijing, China, October 12–16, 1999.

[21] A. Collys, Economische en Energetische Vergelijking van Alternatieve Energiebronnen Voor Elektrische en Hybride Voertuigen, Final Report, Contract Nr. 95, Ministerie van Economische zaken, Vrije Universiteit Brussel, Belgium, July 1997.

[22] Eledrive, Thematic network on fuel cell, electric and hybrid vehicles, coordinated by AVERE, funded by the EC.

[23] H. Kahlen, Energy and power from supercapacitors and electrochemical sources, in: Proceedings of the EVS-16, EVAAP, Beijing, China, October 1999.

[24] Secondary batteries for the propulsion of road vehicles, Part 3, performance and life testing (traffic compatible, urban use vehicles), International standard IEC 61982-3:2001.

[25] Lead acid traction batteries for road vehicle and industrial truck applications, IEC 60254-1:1997, Section 4.2.7.

[26] L.A.M. Van Dongen, Energetische Optimalisatie van Aandrijfsystemen Voor Elektrische Voertuigen, Thesis, Technische Hogeschool Eindhoven, The Netherlands, March 1983.

[27] C.C. Chan, E.W.C. Lo, S. Weixiang, An overview of battery technology in electric vehicle, in: Proceedings of the EVS-16, EVAAP, Beijing, China, October 1999.

[28] H. Kahlen, B. Hauck, Leistung und Leistungsdichte von Traktionsbatterien, Elektrische Bahnen 90, Germany, December 1992.

[29] U. Zoelch, D. Schroeder, Comparison of electric drives for a hybrid vehicle, in: Proceedings of the EPE-95, European Power Electronics and Drives Association, Sevilla, Spain, 1995.

[30] F. Brucchi, Ultracapacitor tests for EV applications: introduction of new equalisation coefficients, in: Proceedings of the EVS-16, EVAAP, Beijing, China, October 1999.

[31] Department of Energy (DOE) Hybrid Vehicle Propulsion Program On-line Resource Center brought by the National Renewable Energy Laboratory (NREL). http://www.hev.doe.gov/components/ultra.html.

[32] P. Chapoulie, S. Astier, Modeling of an electric vehicle including ultracapacitor with saber, in: Proceedings of the EVS-15, AVERE, Brussels, Belgium, October 1998.

[33] J. Swann, Reduced energy consumption and environmental impact from road vehicles through the development and implementation of simulation tools, Technical Report TR3 of WP3 Systems modelling, Fleets Energy Programme, JOULE (JOE3960031), Motor Industry Research Association Ltd., Nuneaton, Warwickshire, UK, 1998.

[34] Department of Energy (DOE) Hybrid Vehicle Propulsion Program On-line Resource Center brought by the National Renewable Energy Laboratory (NREL). http://www.hev.doe.gov/components/flywheels.html.

[35] F.J.M. Thoolen, Development of an advanced high speed flywheel energy storage system, Ph.D. Thesis, Technische Universiteit Eindhoven, The Netherlands, December 1993.

[36] M. Hemmingsson, Minimization of energy losses in hybrid electric vehicles, theory and practice, in: Proceedings of the EVS-16, EVAAP, Beijing, China, October 1999.

[37] Cadastre des Emissions Gaseuses, Final Report, Contract IBGE nr. 139, Institut Bruxellois pour la gestion de l'environnement, STRATEC, Brussels, Belgium, February 1994.

[38] E. Sérié, R. Joumard, Modelling of cold start emissions for road vehicles, Report LEN 9731, INRETS, Bron, France, December 1997.

[39] M. Keller, P. de Haan, Intermodal comparisons of atmospheric pollutant emissions, MEET project, Deliverable no. 24, EC Contract No. ST-96-SC.204, INFRAS, Berne, Switzerland, October 1998.